CHEMISTRY OF MATERIALS

Article

pubs.acs.org/cm

Mercury Nanodrops and Nanocrystals

G. V. Ramesh, Muvva D. Prasad, and T. P. Radhakrishnan*

School of Chemistry, University of Hyderabad Hyderabad, 500 046, India

Supporting Information

ABSTRACT: Directed synthesis of stable mercury nanodrops and nanocrystals and exploration of their characteristic attributes are outstanding challenges, with the potential to unveil a new family of nanomaterials. The unique status of mercury among the chemical elements and metals, in particular, underlines the significance and perhaps explains the absence of any reports, so far, of such studies. A facile and simple protocol is developed for the generation of stable mercury nanodrops inside a polymer thin film, exploiting the *in situ* chemical reduction of precursor ions by the polymer itself under mild thermal annealing. The films exhibit the localized surface plasmon resonance absorption predicted for nano-mercury. Nanocrystals formed by freezing the nanodrops are observed directly and characterized using cryo-transmission electron microscopy and selected area electron diffraction of the free-standing nanocomposite thin film. Size dependence of the melting temperature is established by monitoring the electron diffraction in a variable-temperature experiment. Melt−freeze cycling reveals significant hysteresis effects. The mercury−polymer nanocomposite thin film is found to exhibit visible photoluminescence.

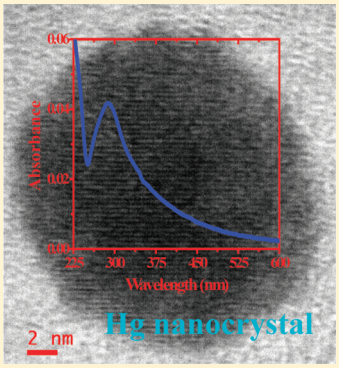

KEYWORDS: *mercury nanocrystals, mercury nanodrops, photoluminescence, polymer, thin film*

INTRODUCTION

Metal nanoparticles have been at the focus of extensive explorations and the basis of numerous technological applications, from the ancient to the modern days, and are poised to play a vital role in futuristic developments. The bulk of the investigations relate to metals such as silver and gold, followed by other noble metals and transition/rare earth metals. In spite of its special status among metallic elements, mercury is conspicuous by the paucity of investigations on its nano-forms. The physical state of mercury under ambient conditions preempts the use of most of the protocols commonly employed for nanomaterials fabrication. Studies on colloidal amalgams have examined the impact of alloying with mercury on silver and gold nanoparticles.[1−3] The calculated UV−visible absorption spectrum of nanoscale mercury,[4] attributable to the localized surface plasmon resonance (LSPR), has been observed in colloids formed by ultrasonic dispersion[5] and chemical reduction,[1,2] but stable mercury nanoparticles were not identified in these studies. Partial reduction of mercury(II) oxide nanoparticles inside a polyethylene matrix was shown to conserve the morphology of the particles,[6] although the product nanostructures and their characteristics were not established. A low-temperature X-ray diffraction study showed that the large (250 nm−20 μm) particles of mercury formed via the decomposition of dimethyl mercury inside a carbon shell had the rhombohedral structure of mercury crystal;[7] no nanocrystal characteristics were reported. Cubic particles observed in the cryo-TEM image of plasmid DNA treated with mercury(II) ions have been attributed to mercury nanocrystals but not investigated further.[8,9] A liquid metal (Hg)−solid semiconductor (HgS) heterostructure has a mercury head ∼500 nm in diameter, showing bulk characteristics.[10]

Melting temperatures of metal[11−16] and semiconductor[17−19] nanoparticles are generally lower than that of the corresponding bulk materials and are size-dependent. The melting and freezing of nanoparticles and the associated hysteresis effects have been investigated using a variety of techniques such as electron microscopy,[20] X-ray scattering,[21] calorimetry,[22] optical reflectance,[23] and LSPR absorption,[24] as well as simulation studies.[25−27] Even though the melting and freezing of mercury trapped in nanoporous glass have been studied using neutron diffraction and calorimetry,[28] as well as acoustic techniques,[29,30] direct electron microscopy characterization of stable mercury nanostructures and their solid−liquid transition have not been reported.

As seen from the overview above, no directed synthesis of stable nano-forms of elemental mercury is known. Neither has there been a systematic characterization of mercury nanostructures nor a direct observation of their size-dependent and potentially unique characteristics. Such explorations are of fundamental interest in the nanoscience of metals, possibly unraveling novel materials applications as well. The unique physical attributes of mercury make it convenient as well as significant to investigate the basic issue of its melting and freezing transitions at the nanoscale. Mercury is known to show anomalous behavior when confined to one dimension.[31,32] Zero dimensional nanostructures of mercury could manifest novel

Received: August 2, 2011
Revised: October 8, 2011
Published: November 14, 2011

dx.doi.org/10.1021/cm2022533 | *Chem. Mater.* 2011, 23, 5231−5236

characteristics. The LSPR absorption of mercury is of potential interest in photonics related and sensing applications.

Several protocols are available for the *in situ* generation of metal nanoparticles inside polymer thin films.[33] The simple thermal annealing procedure that we have optimized has been used to fabricate poly(vinyl alcohol) (PVA) thin film with embedded silver nanoparticles,[34] gold nanoplates[35] and palladium nanowires;[36] the growth of silver nanoparticles inside poly(vinylpyrrolidone) thin film was monitored in real time.[37] Optical,[34,38] electronic,[39] microwave,[40] patterning,[41] catalysis,[42] and sensor[43] applications of the silver nanoparticle–embedded polymer films have been demonstrated. In the *in situ* technique, the polymer with its hydroxyl groups acts as the reducing agent for the metal ions, as well as the stabilizer for the nanostructures generated. Use of a sacrificial layer of polystyrene facilitates the fabrication of very thin free-standing films that can be imaged directly in a TEM.[34−37] These developments allowed us to formulate a new approach to the fabrication and exploration of nano-mercury.

In this article, we describe the fabrication of mercury nanodrops within a PVA film using the *in situ* process and their condensation to nanocrystals in a cryo-TEM experiment. The nanodrops and nanocrystals are characterized in detail using optical absorption and emission spectroscopy as well as electron microscopy, including electron diffraction. Size dependence of the melting of mercury nanocrystals and the hysteresis observed in the melt–freeze cycles are investigated, followed by preliminary exploration of the visible photoluminescence of the Hg–PVA nanocomposite thin film.

EXPERIMENTAL SECTION

Fabrication of Hg–PVA Thin Film. 78.5 mg of mercury(I) nitrate dihydrate (Merck, 97%) was dissolved in 1.0 mL of ∼0.47 N aqueous nitric acid and mixed with 0.5 mL of a solution of poly(vinyl alcohol) (PVA; Aldrich, average molecular weight = 13−23 kDa, % hydrolysis = 87−89) in water (3.6 g PVA dissolved in 16 mL of water with mild heating); the resulting weight ratio of Hg/PVA is 0.50. The solution mixture was stirred for 10 min at 25 °C. Millipore Milli-Q water (resistivity = 18 MΩ cm) was used in all operations. Glass and quartz substrates were cleaned in soap solution and water followed by sonication with isopropyl alcohol for 10 min and dried in a hot air oven. The $Hg_2(NO_3)_2$–PVA solution was spin-coated on the substrate at 500 rpm for 10 s followed by 8000 rpm for 10 s; a Laurell Technologies Corporation model WS-400B-6NPP/LITE/8K Photoresist spinner was used. The film was heated in a hot air oven under different conditions of temperature (60−110 °C) and time (1−3 h). Thickness of the films was measured using an Ambios Technology XP-1 profilometer.

Mercury Content Analysis. A film of known area and thickness fabricated as described above was dissolved in concentrated HNO_3 and diluted with water. The concentration of mercury in the solution was determined using inductively coupled plasma-optical emission spectrometer (ICP-OES, Varian model Liberty series). An Hg–PVA film (4 mL solution) with the dimensions 2.50 cm × 2.50 cm × 125 nm gave an Hg concentration of 2.26 μg/mL. The weight of Hg in the film, estimated from this is 9.04 μg. Based on the density of Hg (13.6 g cm^{-3}), this accounts for a volume of 6.65×10^{-7} cm^3. As the total volume of the film is 7.81×10^{-5} cm^3, the volume of the PVA matrix is 7.74×10^{-5} cm^3 and its weight is 96.8 μg (average density of PVA = 1.25 g cm^{-3}). Therefore, the Hg/PVA weight ratio is 0.0934. ICP-OES analysis of the unheated film gave a mercury concentration of 12.1 μg/mL; this implies an Hg/PVA weight ratio of 0.520, consistent with the ratio in the initial mixture. Partial loss through evaporation accounts for the lower Hg/PVA ratio in the heated film.

Spectroscopy. Optical absorption spectra of films coated on quartz plates were recorded on a Varian Cary 100 spectrometer in transmission mode. Fluorescence spectra of the films were recorded on a Horiba Jobin Yvon model FL3-22 Fluorolog spectrofluorimeter. To avoid any interference due to possible fluorescence from the substrate, a free-standing film was used in these studies, prepared as described for the electron microscopy samples below. To facilitate the peeling, the film had to be thicker than what was used in the other studies; therefore, a higher content of PVA was used (Hg/PVA = 0.16). Fluorescence lifetime was probed using the time-domain technique with a MicroTime 200 instrument (PicoQuant) and images recorded using an Olympus IX71 microscope (PicoQuant). Excitation was achieved using a 405 nm pulsed laser diode, and the fluorescence observed through a 430 nm long pass filter. The fwhm of the pulse response function was 176 ps.

Microscopy. Transmission electron microscopy was carried out on an FEI TECNAI G^2 S-Twin TEM at accelerating voltages of 120 and 200 kV. A Gatan model 900 Smartset cold stage temperature controller and a Gatan model 629 DH cryotransfer specimen holder were used in the cryo-experiments. To prepare extremely thin films for TEM imaging, the substrate was prepared by first spin-coating a few drops of a solution of 1 g of polystyrene (PS, average molecular weight = 280 kDa) in 8 mL of toluene at 1000 rpm for 10 s, followed by drying in a hot air oven at 85−90 °C for 20 min.[34] A thin film of $Hg_2(NO_3)_2$–PVA was coated on top of the PS layer by spinning at 500 rpm for 10 s followed by 8000 rpm for 10 s and subsequently heated. A small portion of the film was then cut and peeled off the glass, placed on a 200 mesh carbon coated copper grid and dipped in toluene, whereupon the PS layer alone dissolved out. Scanning electron microscopy was carried out using a Zeiss Ultra 55 field emission SEM with Oxford INCA X-Act energy dispersive spectroscopy system. The samples were prepared by fabricating the Hg–PVA film on an ITO-coated glass plate and imaged at ambient temperature. Scanning confocal fluorescence images were recorded on a Leica TCS SP2 AOBS DM6000 B upright confocal microscope (λ_{exc} = 250−360 nm; λ_{em} = 400−700 nm).

Simulations. Simulation of the nanocluster was carried out using Materials Studio program.[44] The structure was constructed using the reported crystal structure of mercury (space group no. 166; a = 2.9925 Å and α = 70.743°)[45] as the input. The sequence of options, "Build", "Nanostructure", "Nanocluster", and "Sphere" were used. The desired radius of 90 Å was imposed, and the cluster was rotated so that it could be viewed along the preferred direction. The selected area electron diffraction (SAED) pattern was simulated using the web-based electron microscopy application software, Web-EMAPS.[46]

RESULTS AND DISCUSSION

The standard reduction potentials of mercury ($E^{\circ}_{Hg_2^{2+}/Hg}$ = +0.80 V; $E^{\circ}_{Hg^{2+}/Hg}$ = +0.85 V) and silver ($E^{\circ}_{Ag^{+}/Ag}$ = +0.7996 V) and the observed reduction of Ag^+ by PVA[34] suggest that it should be possible for PVA to reduce mercury ions; overpotential effects may be relevant, as has been pointed out for the polyol reduction of metal ions.[47] Our experiments showed that both mercury(I) and mercury(II) ions are suitable precursors; studies with the former are presented here. Aqueous solutions of $Hg_2(NO_3)_2{\cdot}2H_2O$ and PVA were mixed in suitable proportions and spin-coated on glass/quartz plates, as described in the Experimental section. After drying in air, the film was heated in an oven, leading to the generation of mercury nanodrops inside. Based on several trial experiments, the optimal parameters identified are 110 °C for 60 min with the film having an initial Hg/PVA weight ratio of 0.5. As noted earlier, the final film has an Hg/PVA ratio of ∼0.1, reflecting a partial loss of mercury during the thermal treatment. The transparent Hg–PVA films formed are 120−150 nm thick (Supporting Information, Figure S1). Optical absorption spectra show clear changes upon heating the film; the absorption band with λ_{max} at 253 nm due to the precursor nearly disappears, and a well-defined peak with λ_{max} at 287 nm

dx.doi.org/10.1021/cm2022533 | *Chem. Mater.* 2011, 23, 5231−5236

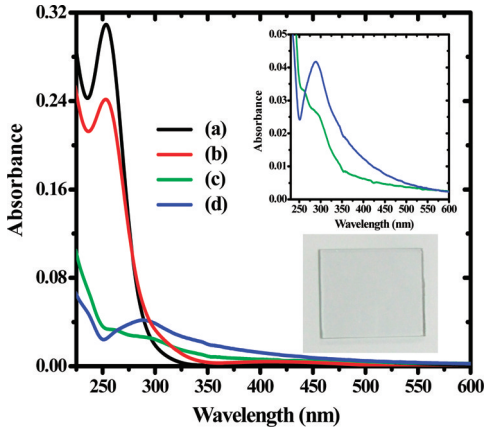

Figure 1. Optical absorption spectra of (a) the unheated precursor $Hg_2(NO_3)_2$–PVA film and the Hg–PVA film obtained by heating at (b) 60 °C, (c) 90 °C, and (d) 110 °C for 60 min. Insets: Enlarged view of spectra (c) and (d) of the Hg–PVA films revealing clearly the LSPR absorption; photograph of the Hg–PVA film on a glass substrate.

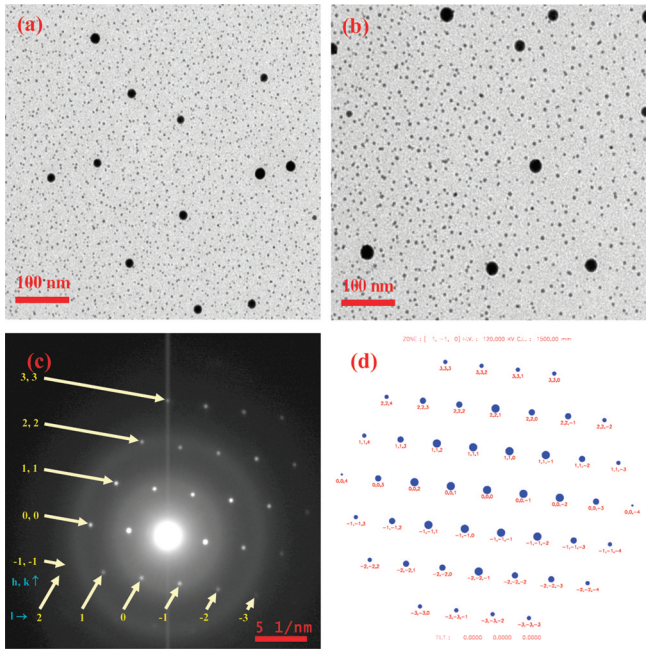

Figure 2. TEM images of Hg–PVA film at (a) 23 °C and (b) −120 °C respectively. (c) Selected area electron diffraction from one nanocrystal at −120 °C; indexing of the spots is shown based on the simulation in (d).

emerges (Figure 1; see also Figures S2 and S3 in the Supporting Information). The latter value is in good agreement with the computed optical absorption of nanoscale mercury with λ_{max} at ∼280 nm.[4]

TEM images of free-standing Hg–PVA films fabricated using a sacrificial polystyrene layer, as described in the Experimental section, were recorded with a 120 kV electron beam and typical beam currents of 1.5 μA. The image obtained at the ambient temperature of 23 °C is shown in Figure 2a (see also Figure S4 in the Supporting Information). As expected, the nanodrops (nanoparticles in the liquid phase) yield no electron diffraction spots; they are found to evaporate under the electron beam, revealing a characteristic meniscus during the process (Supporting Information, movie). However, the Hg–PVA

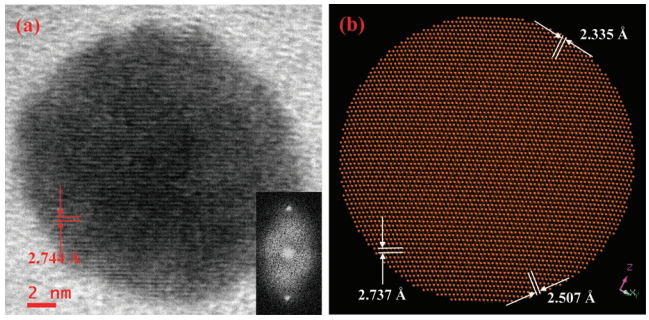

Figure 3. (a) High resolution TEM image of one Hg nanocrystal in an Hg–PVA film at −120 °C; the interplanar spacing calculated from the fast Fourier transform of the image (inset) is indicated. (b) Model of an 18 nm diameter cluster generated from Hg crystal lattice, viewed along the [1$\bar{1}$0] direction; interplanar distances are indicated.

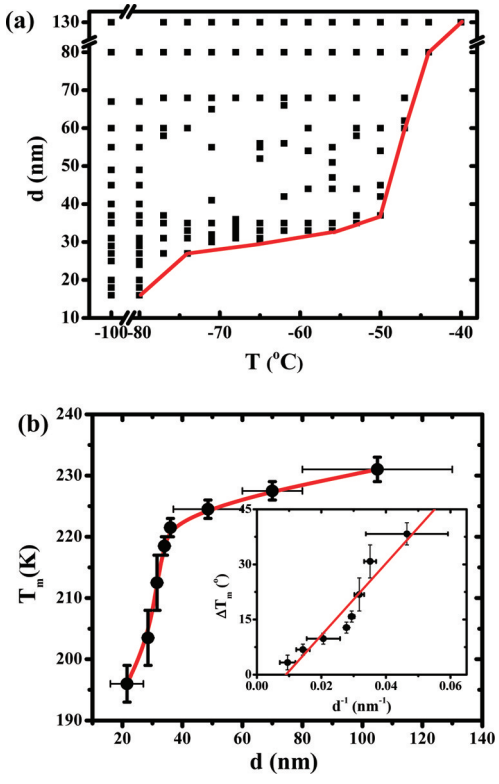

Figure 4. (a) Range of sizes (diameter, d) of Hg nanocrystals observed in the Hg–PVA film at different temperatures, T. (b) Plot of the melting temperature, T_m, of the nanocrystals against the particle diameter, d; the line is only a guide to the eye. Inset: plot of the depression in melting temperature (ΔT_m) of the nanocrystals against the inverse of the particle diameter and the least-squares fit line.

film is very stable under the ambient conditions in the laboratory with little change occurring even after a year (Supporting Information, Figure S5); this stability is reassuring from the point of view of toxicity concerns that could arise while considering potential applications of the Hg–PVA film. Chemical identity of the nanodrops was confirmed using field emission scanning electron microscopy with energy dispersive spectroscopy (Supporting Information, Figure S6).

To freeze the nanodrops to nanocrystals, the film was cooled at a rate of 3 °C/min. The image recorded at −120 °C is shown in Figure 2b; at this temperature, the nanocrystals are very stable under the beam over extended periods of time (>1 h).

dx.doi.org/10.1021/cm2022533 | *Chem. Mater.* 2011, 23, 5231–5236

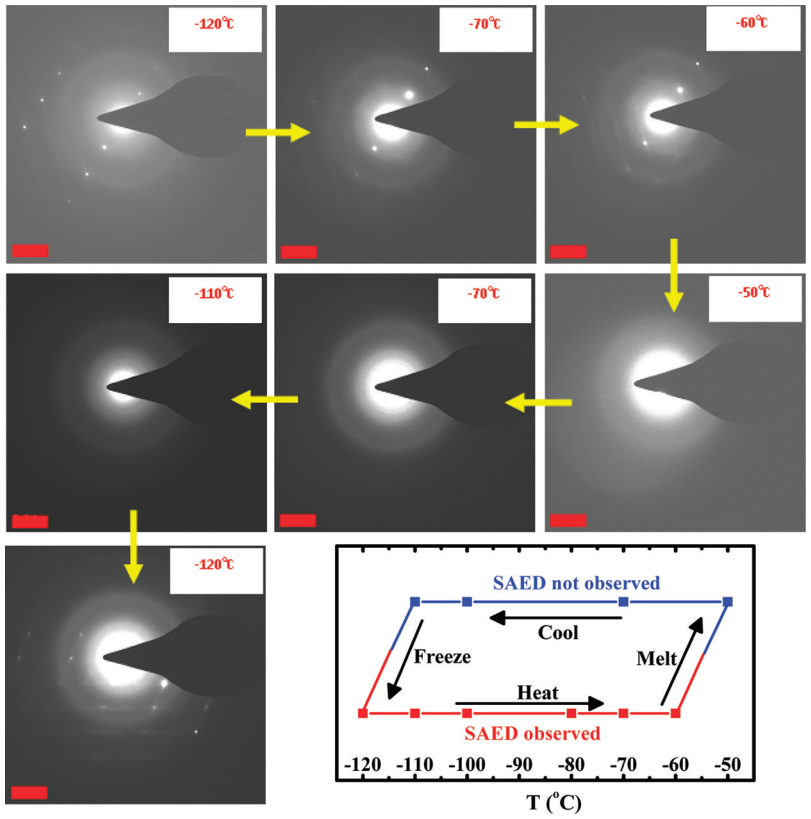

Figure 5. SAED pattern of a single Hg nanoparticle (55 nm diameter) in the Hg–PVA film at selected temperatures in a melt–freeze cycle (full cycle is shown in Figure S15 in the Supporting Information); scale bar = 5 nm^{-1}. Schematic representation of the presence or absence of the SAED during the cycle is also shown (the error in the temperatures is typically ±3 °C).

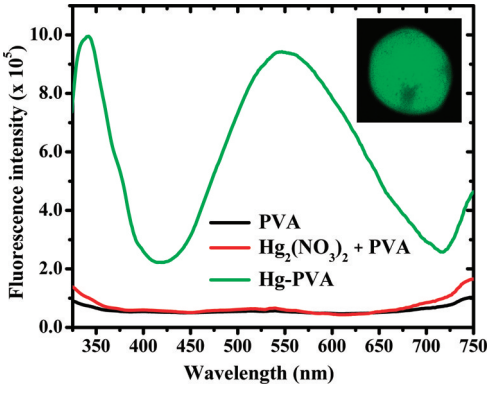

Figure 6. Fluorescence emission spectra (λ_{exc} = 290 nm) of free-standing films of PVA, $Hg_2(NO_3)_2$–PVA (without heating), and Hg–PVA (heated at 110 °C for 60 min). Inset: laser confocal fluorescence image of a piece of the Hg–PVA film (λ_{exc} = 250–360 nm).

More significantly, the SAED pattern could be recorded on individual nanostructures with sizes typically ≥15 nm; dark field images confirm the origin of the diffraction (Supporting Information, Figure S7). The diffraction pattern shown in Figure 2c is indexed to rhombohedral mercury crystal with the unit cell reported earlier[45] and [1$\bar{1}$0] zone axis (Figure 2d; see also Figure S8 in the Supporting Information).[46] Several individual crystals examined showed the same crystal structure but different zone axes (Supporting Information, Figures S9 and S10). Control experiments with a pure PVA film and the unheated PVA film containing the precursor salt (Supporting Information, Figures S11 and S12) prove unambiguously that these diffractions originate from the mercury nanocrystals. High resolution image of a nanocrystal recorded using a 200 kV electron beam is shown in Figure 3a. It reveals the interplanar spacing of 2.744 Å (Supporting Information, Figure S13) consistent (within experimental error) with the simulation of a nanocluster viewed along [1$\bar{1}$0] (Figure 3b); the smaller interplanar spacings are not resolved in the image.

In situ TEM analysis is a powerful technique to study phenomena such as melting,[11,16,17,48,49] shape evolution,[50,51] and solid state diffusion[52] at the nanoscale. The facile access to the melting transition of mercury in a cryo-TEM coupled with the fabrication of a thin film containing stable mercury nanodrops of various sizes, opened up the opportunity to conveniently probe the fundamental issue of size effect on the melting temperature. Even though this could be accomplished in a single experiment, to establish the consistency of the observations, data from several experiments were accumulated. TEM images and electron diffraction of the mercury nanostructures were monitored while heating the film from −120 to −35 °C. After stabilizing at each temperature, different areas of the film were examined and SAED from individual structures of different sizes were collected (Supporting Information, Figure S14). Crystals of all sizes are found to be stable up to ∼−80 °C, exhibiting clear electron diffraction; subsequently, the lower limit of the size of nanocrystals observed at any temperature rises with the temperature. Figure 4a shows the sizes of particles exhibiting electron diffraction at each temperature; in other words, the data points represent the range of sizes of stable mercury nanocrystals observed at each temperature. Size dependence of the melting of mercury nanocrystals inferred from this data is shown graphically in

dx.doi.org/10.1021/cm2022533 | *Chem. Mater.* 2011, 23, 5231–5236

Figure 4b; the trend is consistent with general theoretical expectations.[12] It is qualitatively similar to that reported earlier on the basis of an acoustic study of melting and freezing of mercury nanoparticles confined inside porous glass.[30] However, there are quantitative differences; we find that the radii of particles exhibiting melting point decreases of ~20−40° are in the range 25−10 nm, whereas the corresponding range in the earlier study is 10−5 nm. The particle sizes estimated based on the pore size distribution of the glass matrix may be less accurate than those directly observed now. It is important to consider the extent to which the melting may be influenced by electron beam heating in the TEM. With the low beam current and voltage used, it is likely to be negligible. To confirm this, as the temperature rise is expected to be proportional to the beam current,[53] we have carried out the experiment with a current 2.5 times higher, that is, 3.8 μA, with the voltage kept at 120 kV; melting temperatures for the different sizes are found to remain the same within experimental error, ruling out possible interference due to beam heating.

We have probed the solid−liquid transition further by monitoring the melt−freeze cycles of individual nanostructures. The large hysteresis in the disappearance and reappearance of the SAED from a single nanoparticle is evident in the selected patterns, and the schematic diagram shown in Figure 5 (see also Figure S15 in the Supporting Information). The hysteresis is likely due to the kinetic factors involved in the nucleation process. Even though there is no direct evidence available at the moment, the possibility of the diffusion of mercury atoms into the polymer matrix upon melting and the consequent barrier to crystallization upon cooling cannot be ruled out. The freezing temperatures vary relatively less with the size of the nanodrop; the hysteresis decreases with decrease in particle size (Supporting Information, Figure S16). Decreasing hysteresis at smaller sizes has been reported in bismuth[21] and lead[23] nanoparticles. It is notable that a classical thermodynamic treatment including the effects of surface-induced order has predicted an energy barrier between surface melted state and the liquid droplet that decreases with particle size, causing the melt−freeze hysteresis also to decrease and vanish at very small sizes.[54] Decrease of hysteresis with particle size has been discussed in connection with first-order crystallographic phase transitions, as well.[55] Finally, we note that the SAED experiment on pure PVA film showed no hysteresis (Supporting Information, Figure S11).

Atomic emission lines of mercury occur across the UV and blue−green region. To the best of our knowledge, bulk mercury does not show any visible fluorescence. Hg−PVA nanocomposite thin film at ambient temperature is found to exhibit visible photoluminescence. The emission spectrum of a free-standing film (Figure 6) excited at 290 nm shows a peak at ~345 nm and a broad emission with maximum at 550 nm; there is no contribution from PVA or the precursor salt as shown by their spectra. The excitation spectrum for the emission at 550 nm shows peaks at 305, 365, and 425 nm (Supporting Information, Figure S17); the localized surface plasmon state is likely to be one of the origins of the emission. Fluorescence lifetime based imaging of the film indicates an average excited state lifetime of ~1.4 ns (Supporting Information, Figure S18). Laser scanning confocal fluorescence image and the corresponding spectrum are consistent with the emission spectrum in Figure 6 (Supporting Information, Figure S19). The current observations indicate that the visible emission results from the mercury nanostructures. Emission from metal clusters is well established;[56] therefore, it is likely that the fluorescence observed in the Hg−PVA film arises from the small mercury nanodrops. It may be noted that, as a result of the lower Hg/PVA ratio used in the fabrication of these films, the nanodrops are likely to be smaller than those shown in Figure 1 (Supporting Information, Figure S4).

■ CONCLUSIONS

The present study establishes, for the first time, a simple protocol for the direct synthesis of stable mercury nanodrops by *in situ* reduction of mercury ions inside poly(vinyl alcohol) film by the polymer itself. Nanocrystals are formed by freezing the nanocomposite thin films and characterized in detail using cryo-TEM and SAED. The thin film samples containing mercury nanocrystals of different sizes facilitated convenient demonstration of the size-dependence of the melting transition; the solid−liquid transition of nano-mercury in the polymer matrix shows large hysteresis. The nanocomposite thin films exhibit broad visible photoluminescence. Stability of the nano-mercury embedded within the polymer matrix demonstrated in the present study suggests that the optical and mechano-electrical properties of the nanocomposite films could form the basis for various applications in photonics and electronics. One hundred years since the discovery of superconductivity in bulk mercury, fundamental questions related to the case of nano-mercury remain. The current study opens up the opportunity to explore a new family of nanomaterials based on mercury and its unique attributes.

■ ASSOCIATED CONTENT

Ⓢ Supporting Information

Details of film fabrication and characterization, optical absorption and fluorescence spectroscopy, transmission electron and scanning electron microscopy, electron diffraction, and control experiments. This material is available free of charge via the Internet at http://pubs.acs.org.

■ AUTHOR INFORMATION

Corresponding Author

*Fax: 91-40-2301-2460. Phone: 91-40-2313-4827. E-mail: tprsc@uohyd.ernet.in, tprsc1@gmail.com.

■ ACKNOWLEDGMENTS

Financial support from the DST, New Delhi, infrastructure support from the Centre for Nanotechnology at the University of Hyderabad, and a senior research fellowship for G.V.R. from CSIR, New Delhi, are gratefully acknowledged. We thank Mr. E. Manohar Reddy and Mr. M. Lakshminarayana for help with the microscopy work.

■ REFERENCES

(1) Katsikas, L.; Guttiérrez, M.; Henglein, A. *J. Phys. Chem.* **1996**, *100*, 11203−11206.
(2) Henglein, A.; Brancewicz, C. *Chem. Mater.* **1997**, *9*, 2164−2167.
(3) Henglein, A.; Giersig, M. *J. Phys. Chem. B.* **2000**, *104*, 5056−5060.
(4) Creighton, J. A.; Eadon, D. G. *J. Chem. Soc. Farad. Trans.* **1991**, *87*, 3881−3891.
(5) Shafeev, G. A.; Bozon-Verduraz, F.; Robert, M. *Phys. Wave Phenom.* **2007**, *15*, 131−136.
(6) Gorkovenko, M. Y.; Yurkov, G. Y.; Buslaeva, E. Y.; Gubin, S. P. *Russ. J. Inorg. Chem.* **2006**, *51*, 51−56.
(7) Luvchik, E.; Calderon-Moreno, J. M.; Veglio, N.; Tamarit, J. L. I.; Gedanken, A. *Adv. Mater.* **2008**, *20*, 1000−1002.

(8) Majumdar, S.; Priyadarshini, M.; Subudhi, U.; Chainy, G. B.N.; Varma, S. *Appl. Surf. Sci.* **2009**, *256*, 438−442.
(9) Majumder, S.; Priyadarshini, M.; Subudhi, U.; Umananda, M.; Chainy, G. B. N.; Satyam, P. V.; Varma, S. *Appl. Phys. Lett.* **2009**, *94*, 073110−3.
(10) Wu, L.; Quan, B.; Liu, Y.; Song, R.; Tang, Z. *ACS Nano* **2011**, *5*, 2224−2230.
(11) Coombes, C. J. *J. Phys. F* **1972**, *2*, 441−449.
(12) Buffat, Ph.; Borel, J. -P. *Phys. Rev. A* **1976**, *13*, 2287−2298.
(13) Lai, S. L.; Guo, J. Y.; Petrova, V.; Ramanath, G.; Allen, L. H. *Phys. Rev. Lett.* **1996**, *77*, 99−102.
(14) Dippel, M.; Maier, A.; Gimple, V.; Wider, H.; Evenson, W. E.; Rasera, R. L.; Schatz, G. *Phys. Rev. Lett.* **2001**, *87* (095505), 1−4.
(15) Olson, E. A.; Efremov, M.Yu.; Zhang, M.; Zhang, Z.; Allen, L. H. *J. Appl. Phys.* **2005**, *97* (034304), 1−9.
(16) Mei, Q. S.; Lu, K. *Prog. Mater. Sci.* **2007**, *52*, 1175−1262.
(17) Goldstein, A. N.; Echer, C. M.; Alivisatos, A. P. *Science* **1992**, *256*, 1425−1427.
(18) Goldstein, A. N. *Appl. Phys. A: Mater. Sci. Process.* **1996**, *62*, 33−37.
(19) Hirasawa, M.; Orii, T.; Seto, T. *Appl. Phys. Lett.* **2006**, *88* (093119), 1−3.
(20) Haro-Poniatowski, E.; de Castro, M. J.; Navarro, J. M. F.; Morhange, J. F.; Ricolleau, C. *Nanotechnology* **2007**, *18* (315703), 1−7.
(21) Kellermann, G.; Craievich, A. F. *Phys. Rev. B* **2008**, *78* (054106), 1−5.
(22) Unruh, K. M.; Huber, T. E.; Huber, C. A. *Phys. Rev. B* **1993**, *48*, 9021−9027.
(23) Cheyssac, P.; Kofman, R.; Garrigos, R. *Phys. Scr.* **1988**, *38*, 164−168.
(24) Schwind, M.; Zhdanov, V. P.; Zoric, I.; Kasemo, B. *Nano Lett.* **2010**, *10*, 931−936.
(25) Shao, J.; Yang, C.; Zhu, X.; Lu, X. *J. Phys. Chem. C* **2010**, *114*, 2896−2902.
(26) Shi, R.; Shao, J.; Zhu, X.; Lu, X. *J. Phys. Chem. C* **2011**, *115*, 2961−2968.
(27) Sdobnyakov, N. Y.; Komarov, P. V.; Sokolov, D. N.; Samsonov, V. M. *Phys. Met. Metallogr.* **2011**, *111*, 13−20.
(28) Kumzerov, Y. A.; Nebereznov, A. A.; Vakhrushev, S. B.; Savenko, B. N. *Phys. Rev. B* **1995**, *52*, 4772−4774.
(29) Borisov, B. F.; Charnaya, E. V.; Plotnikov, P. G.; Hoffmann, W. D.; Michel, D.; Kumzerov, Y. A.; Tien, C.; Wur., C. S. *Phys. Rev. B* **1998**, *58*, 5329−5335.
(30) Borisov, B. F.; Gartvik, A. V.; Nikulin, F. V.; Charnaya, E. V. *Acoust. Phys.* **2006**, *52*, 138−143.
(31) Bogomolov, V. N.; Kolla, E.; Kumzerov, Y. A. *Solid State Commun.* **1983**, *46*, 383−384.
(32) Kim, W. Y.; Nautiyal, T.; Your, S. J.; Kim, K. S. *Phys. Rev. B* **2005**, *71* (113104), 1−4.
(33) Ramesh, G. V.; Porel, S.; Radhakrishnan, T. P. *Chem. Soc. Rev.* **2009**, *38*, 2646−2656.
(34) Porel, S.; Singh, S.; Harsha, S. S.; Rao, D. N.; Radhakrishnan, T. P. *Chem. Mater.* **2005**, *17*, 9−12.
(35) Porel, S.; Singh, S.; Radhakrishnan, T. P. *Chem. Commun.* **2005**, 2387−2389.
(36) Porel, S.; Hebalkar, N.; Sreedhar, B.; Radhakrishnan, T. P. *Adv. Funct. Mater.* **2007**, *17*, 2550−2556.
(37) Ramesh, G. V.; Sreedhar, B.; Radhakrishnan, T. P. *Phys. Chem. Chem. Phys.* **2009**, *11*, 10059−10063.
(38) Meng, X.; Fujita, K.; Zong, Y.; Murai, S. *Appl. Phys. Lett.* **2008**, *92* (20112), 1−3.
(39) Leong, W. L.; Lee, P. S.; Lohani, A.; Lam, Y. M.; Chen, T.; Zhang, S.; Dodabalapur, A.; Mhaisalkar., S. G. *Adv. Mater.* **2008**, *20*, 2325−2331.
(40) Ramesh, G. V.; Sudheendran, K.; Raju, K. C. J.; Sreedhar, B.; Radhakrishnan, T. P. *J. Nanosci. Nanotech.* **2009**, *9*, 261−266.
(41) Abargues, R.; Marqués-Hueso, J.; Canet-Ferrer, J.; Pedrueza, E.; Valdés, J. L.; Jiménez, E.; Martínez-Pastor., J. P. *Nanotechnology* **2008**, *19* (355308), 1−7.
(42) Hariprasad, E.; Radhakrishnan, T. P. *Chem.—Eur. J.* **2010**, *16*, 14378−14384.
(43) Ramesh, G. V.; Radhakrishnan, T. P. *ACS Appl. Mater. Interfaces* **2011**, *3*, 988−994.
(44) Materials Studio 4.3 (Accelrys Software Inc.).
(45) Barrett, C. S. *Acta Crystallogr.* **1957**, *10*, 58−60.
(46) Zuo, J. M.; Mabon, J. C.Web-based Electron Microscopy Application Software: Web-EMAPS. *Microsc. Microanal.* **2004**, *10*,Suppl. 2; Available online: http://emaps.mrl.uiuc.edu/
(47) Boneta, F.; Guéry, C.; Guyomard, D.; Urbina, R. H.; Tekaia-Elhsissen, K.; Tarascon, J.- M. *Int. J. Inorg. Mater.* **1999**, *1*, 47−51.
(48) Wronski, C. R. M. *Brit. J. Appl. Phys.* **1967**, *18*, 1731−1737.
(49) Wang, Z. L. *Adv. Mater.* **2003**, *15*, 1497−1514.
(50) Wang, Z. L.; Petroski, J. M.; Green, T. C.; El-Sayed, M. A. *J. Phys. Chem. B* **1998**, *102*, 6145−6151.
(51) Tang, S.; Zhu, S.; Lu, H.; Meng, X. *J. Solid State Chem.* **2008**, *181*, 587−592.
(52) Holmberg, V. C.; Panthani, M. G.; Korgel, B. A. *Science* **2009**, *326*, 405−407.
(53) Liu, L.; Risbud, S. H. *J. Appl. Phys.* **1994**, *76*, 4576−4580.
(54) Vanfleet, R. R.; Mochel, J. M. *Surf. Sci.* **1995**, *341*, 40−50.
(55) Shirinyan, A. S.; Bilogorodskyy, Y. S.; Wilde, G.; Schmelzer, J. W. P. *J. Phys.: Condens. Matter* **2011**, *23* (245301), 1−6.
(56) Maretti, L.; Billone, P. S.; Liu, Y.; Scaiano, J. C. *J. Am. Chem. Soc.* **2009**, *131*, 13972−13980.